

An Implementation of the Deutsch-Jozsa Algorithm on Molecular Vibronic Coherences Through Four-Wave Mixing: a Theoretical Study

Zsolt Bihary^(a), David R. Glenn^(b), Daniel A. Lidar^(b), and V. Ara Apkarian^(a)

^(a)*Department of Chemistry, University of California, Irvine, California 92697,*

^(b)*Department of Chemistry, 80 St. George St., University of Toronto, Toronto, Ontario M5S 3H6*

Time-Frequency Resolved Coherent Anti-Stokes Raman Scattering (TFRCARS) was recently proposed as a means to implement quantum logic using the molecular ro-vibrational manifold as a quantum register [R. Zadoyan *et al.*, Chem. Phys. **266**, 323 (2001)]. We give a concrete example of how this can be accomplished through an illustrative algorithm that solves the Deutsch-Jozsa problem. We use realistic molecular parameters to recognize that, as the problem size expands, shaped pulses must be tailored to maintain fidelity of the algorithm.

Logic operations for quantum computation (QC) between two or more quantum bits (qubits) have so far been experimentally demonstrated in liquid-state NMR [1], trapped ions [2], and cavity quantum electrodynamics [3]. Recently, Time-Frequency Resolved Coherent Anti-Stokes Raman Scattering (TFRCARS) in the molecular ro-vibronic Hilbert space, was proposed as an alternative approach [4]. Through measurements on room temperature iodine vapor, it was demonstrated that the elements sufficient for executing universal quantum logic, namely, the single qubit rotations and the two-qubit controlled-not gate, are naturally contained in TFRCARS. Here, we give an illustrative example of how such elements can be combined into a useful algorithm. We show how a TFRCARS *interference* experiment can use the molecular vibrational level structure to solve the Deutsch-Jozsa (DJ) problem [5]. The DJ problem has become a benchmark for experimental demonstrations of algorithms on prototypes of quantum computers; having so far been used in NMR [6], linear optics [7], and ro-vibrational molecular wavepackets in a pump-probe experiment [8].

TFRCARS is a four-wave mixing experiment in which a sequence of three non-collinear, short laser pulses (labeled P, S and P') are used to resonantly prepare and manipulate molecular ro-vibronic coherences. The P-pulse acts on a statistical state to prepare the first-order polarization $P^{(1)} = \sum c(\xi, \xi') |\xi\rangle \langle \xi'|$ where ξ represents the rotational, vibrational and electronic quantum indices (j, v, χ). The S and P' pulses then allow manipulation of the coherence through stimulated transitions to sequentially prepare second and third order coherences, consisting of complex superpositions determined by the radiation field. Transform-limited interrogation of the evolving third-order coherence can then be accomplished through the projective measurement of gated detection of the spectrally dispersed third-order polarization, $P^{(3)}$ [4,9,10]. Energy and momentum conservation conditions, enforced through spectral and spatial filtering of $P^{(3)}$, allow its detection without any interference from the incoherent background. The process can be mapped out

as logical operations on the molecular register of eigenstates, by identifying the P pulse as initialize, S and P' pulses as process, and the gate pulse as readout. The approach has several attractive features with regard to QC. Since transitions involve electronic resonances, they can be carried out on fs time scales. A very large ratio of coherence to process time ($> 10^5$) is afforded, even when we allow for decoherence to be determined by the non-fundamental limit of inhomogeneous translational distribution (doppler broadening) at room temperature. Unlike NMR, which aims to manipulate effective pure states, in TFRCARS the signal is only from the polarized subensemble [4]. Very large superpositions, $10^2 - 10^4$ ro-vibrational eigenstates, can be manipulated with precision. Finally, since the signal consists of a coherent radiation beam, information can be transferred effectively and can be used to cascade operations. Small scale CARS-QC experiments, using several qubits, are currently being set up at Irvine. The limited number of qubits and process steps in the presently conceived algorithms, suggest applications in quantum communication [11], and simple quantum information processing tasks, such as quantum privacy amplification and cryptography [12]. Even the simplest of propositions in quantum control of molecules [13] must contend with complications inherent in molecular state structures, such as vibrational level structures imposed by anharmonicity of electronic potential energy surfaces. As such, principles of optimal control will invariably be required in devising pulse shapes tailored for various implementations [14]. We highlight these considerations, by using realistic molecular parameters, intuitively obvious pulse shapes, and a clear computational task of solving the DJ problem.

Algorithm.— The DJ algorithm is one of the first examples of a quantum algorithm exhibiting a speedup compared to classical computers. The algorithm solves the following problem: “There is a finite set $X = \{x_k\}_{k=1}^N$ where N is even, and an unspecified function $f : X \rightarrow \{0, 1\}$ that is promised to be either constant [$f(x_k) = 0$ or $1 \forall k$] or balanced [$f(x_k) = 0$ on exactly half the in-

puts]. Decide with certainty whether f is constant or balanced in the least number of evaluations of f ." The DJ algorithm has been analyzed, e.g., in [15]. We now describe an alternative algorithm for solving the DJ problem, that is optimized for an interference experiment. Let \mathcal{H} be an N -dimensional Hilbert-space, where $N = |X|$. Define a basis in \mathcal{H} in one-to-one correspondence with the elements $x_k \in X: \{|x_1\rangle, |x_2\rangle, \dots, |x_N\rangle\}$. 1) Prepare the equal coherent superposition $|\Psi_1\rangle = \sum_{k=1}^N |x_k\rangle$. 2) Define an operator F_f by its action on the basis elements as: $F_f|x_k\rangle = (-1)^{f(x_k)}|x_k\rangle$. Then: $|\Psi_2\rangle = F_f|\Psi_1\rangle = \sum_{k=1}^N (-1)^{f(x_k)}|x_k\rangle$. 3) Make a projective measurement on $|x_1\rangle$. The output (the signal) becomes:

$$S_N(f) = \langle x_1 | \Psi_2 \rangle = \sum_{k=1}^N (-1)^{f(x_k)} \quad (1)$$

Since $f(x_k)$ is either 0 or 1, the terms in the sum are +1 or -1, respectively. It is clear that for f balanced, the sum contains an equal number of positive and negative terms. The signal in this case is zero. For constant f , all the terms have the same sign, so the absolute value of the signal becomes maximal. The signal therefore distinguishes the two types of functions and hence this modified algorithm performs the same task as the standard algorithm [15]. Furthermore, it too does so using just one f -evaluation [16].

Scheme of proposed experiment.— We now propose a concrete experiment on iodine (I_2) vapor to perform our alternative DJ algorithm. We illustrate the proposal through numerical simulations using accurately known molecular parameters. Vibrational levels represent the basis states $|x_k\rangle$ of $|\Psi_1\rangle$. Fig. 1 shows the iodine potentials for the ground (X) and excited (B) electronic states. We choose pulse widths and processing times < 1 ps, on which time scale the evolution of molecular rotations can be ignored, and therefore, we need only to be concerned with the vibrational levels on each potential. The CARS process is illustrated in Fig. 1 through the relevant time-circuit diagram. Initially, the molecule is in its ground state $|X, 0\rangle$, where the first (second) index denotes electronic (vibrational) quantum numbers. The P (pump) pulse is sufficiently wide spectrally to prepare an equal superposition of $|X, 0\rangle\langle w, B|$ coherences, where w are the vibrational states prepared on the (B) level. This step is the preparation of the equal superposition state $|\Psi_1\rangle$. After a delay, the S (Stokes) pulse arrives. If the delay is an integer multiple of the average vibrational period on the (B) level, the S pulse finds approximately the same equal coherent superposition as that prepared by the P pulse. Anharmonicity of the (B) potential will produce dispersion in the evolving packet. To avoid shaping of the S-pulse to compensate for such a dispersion, we will simply keep the process time short. The S pulse is designed to encode the function f . This is done by phase-shifting its spectral components (colors), corresponding

to individual $|B, w\rangle \rightarrow |X, 4\rangle$ transitions (or x_k), with a phase-mask. We need only consider 0 shifts and π shifts here, i.e., the mask element multiplies the spectral component x_k of the pulse by $(-1)^{f(x_k)}$. A mask with a specific sequence of phase factors $((-1)^{f(x_1)}, \dots, (-1)^{f(x_N)})$ is therefore in one-to-one correspondence with a function f . The S pulse allows the projection of all $|B, w\rangle$ levels onto level $|X, 4\rangle$. After the two pulses the $|X, 0\rangle\langle X, 4|$ vibrational coherence equals the sum of the phase-shifted $|X, 0\rangle\langle w, B|$ coherences. Therefore this corresponds to the application of F_f , i.e., the computation of $|\Psi_2\rangle$. The amplitude of this vibrational coherence can then be measured with a third P' pulse, chosen to be resonant with a single $|B, w'\rangle \leftarrow |X, 4\rangle$ transition. To ensure the purity of this transition, a spectrally narrow, therefore temporally long (psec) pulse is used for P' . Let us summarize the scheme: 1) Preparation: The P pulse prepares the equal coherent superposition. 2) Computation: The phase-masked S pulse performs the F_f operation. 3) Measurement: The $|X, 0\rangle\langle X, 4|$ coherence is measured with the P' pulse. The signal is proportional to the absolute value of the coherence: $A(t) = ||X, 0\rangle\langle X, 4||$. This output characterizes f .

Pulse design.— We require an $|X, 0\rangle \rightarrow |B, w\rangle \rightarrow |X, v'\rangle$ transition scheme with the following properties: a) For the general DJ algorithm w should assume N values. Here we consider for definiteness the case of $N = 4, 8$ (equivalent to two and three qubits). b) The Franck-Condon (FC) overlap between X and B should be as large as possible and roughly constant for all $(0, w)$ and (v', w) pairs, in order to maximize the efficiency of coherent transfer by the pulses. c) By choosing a large frequency shift between the P and S pulses it is guaranteed that the single time-circuit diagram of Fig. 1 describes the CARS process. The following values satisfy the above criteria: $v' = 4$; $w = 20 - 23$ for $N = 4$, and $w = 18 - 25$ for $N = 8$. The product of FC factors characterizes the overall strength of the $|X, 0\rangle \rightarrow |B, w\rangle \rightarrow |X, 4\rangle$ transitions. The product is largest and roughly constant around $w = 22$, which motivates our choice of the w values. In Fig. 2, we show the chosen pulse-shapes for P and S in the frequency domain for $N = 4$. P is broad, covering $w = 20 - 23$. S is red-shifted, and phase-masked. Fig. 2 shows the effect of the $(1, -1, 1, -1)$ mask, corresponding to a balanced function f . A delay time equal to one (B) vibrational period (360 fs) is chosen. The P pulse has a duration of 50 fs.

Simulations.— We use Morse functions for the X and B electronic potentials (see Fig. 1). We calculate the vibrational eigenfunctions on both surfaces using the sinc-DVR method, and obtain the FC factors [17]. The time-evolution is explicitly integrated using the energy-representation. Time-ordering of the P and S pulses was not enforced: contributions from (P,S) and (S,P) sequences were added coherently. Only the Liouville pathway depicted in Fig. 1 was taken into account. No de-

coherence mechanism was included (decoherence, which occurs with $\tau > 10^{-9}$ s, can be neglected on the execution time-scale of 1-2 ps). After the application of the two pulses, the prepared $|X, 0\rangle\langle X, 4|$ vibrational coherence preserves its magnitude A and oscillates with the $(X, 0) - (X, 4)$ beat-frequency. The calculated signal is this magnitude.

Results.— The signal $A(f, \tau)$ as a function of delay-time τ between the P and S pulses was computed for all 2^N different phase-masks (i.e., for all possible different encoded f functions, including those that are neither constant nor balanced). Fig. 3 shows the $N = 4$ signals for a constant and a balanced function. For the constant function (left) the signal is large at integer multiples of the (B) period, while the signal is close to zero for the balanced function (right). This is therefore a clear experimental signature that distinguishes constant from balanced functions. Notice, however, that the signal from the balanced function is not exactly zero. In Fig. 4a, we show the signal $A(f, 1)$ for all 16 different encoded f functions, *vs* $S_4(f)$ [Eq. (1)] (only 8 points are actually shown, since the signal is symmetric in $\pm S_4(f)$). For balanced functions $S_4(f) = 0$, so they should yield zero signal. For the two constant functions $|S_4(f)| = 4$, so they should give maximal signal. For the other functions $|S_4(f)| = 2$, so they should give half the signal amplitude. In reality, as expected from Fig. 3, there is a spread along the signal axis, indicating, e.g., that not all balanced functions yield exactly zero signal. Fig. 4b shows the results for $N = 8$ case. Here the spread of signals corresponding to the same class of functions is significantly larger, thus decreasing the fidelity of distinguishing constant *vs* balanced functions. It is useful to introduce a formal fidelity measure in order to quantify the performance of the algorithm. Perhaps the simplest measure is the distinguishability D , which we define as the ratio of signal strengths

$$D = 1 - \frac{\max A(f_{\text{bal}})}{A(f_{\text{con}})}, \quad (2)$$

where the maximum is taken over all balanced signals. In the ideal case all $A(f_{\text{bal}}) = 0$ so $D = 1$. A second measure is the Pearson’s correlation coefficient r for a straight line interpolation between the signal $A(f, \tau)$ and $|S_N(f)|$, which also accounts for the spread in the other (neither constant nor balanced) functions. This measure is important in case one decides to use our algorithm to also distinguish these other functions. In Table 1 we present these fidelities for different N values and for different delay times. The reasons leading to a degradation in fidelity are the following: I) Non-uniform FC factors, causing different $|x_k\rangle$ to be transferred with slightly different amplitude by the P and S pulses. II) Spectral breadth of the laser-pulses, with the same consequence as I). These effects lead to non-uniformity in the prepared and projected coherent superpositions, thus misrepresenting $|\Psi_1\rangle$

and $|\Psi_2\rangle$ somewhat. III) Anharmonicity of the (B) potential, leading to wavepacket dispersion on both the X and B potentials. In order to explore these effects, we performed simulations for the $N = 8$ case, where all FC factors were artificially set equal (a pulse achieving this effect can in principle be shaped by amplitude masking), and the P pulse was spectrally broadened, by reducing its duration to 10 fs. We refer to this as the “tailored” case. The results are presented in Fig. 4c, and the improvement in distinguishability is remarkable. This convincingly demonstrates the role of the non-uniform superposition in fidelity degradation. The solution, a spectrally broader P pulse together with tailoring the *amplitudes* of the P and S pulses to compensate for the non-uniformity of the FC factors, greatly improves the fidelity of the algorithm. To test the role of anharmonicity we also performed simulations at delays $\tau = 0, 2\tau_B$. Obviously, at zero delay anharmonicity cannot play a role. On the other hand anharmonicity should be more significant at $\tau = 2\tau_B$ than at $\tau = \tau_B$. These expectations are confirmed in Table 1: a significant improvement in fidelity is seen when comparing the bare $N = 8$ results to the tailored results, but only for $\tau = 0, 1\tau_B$. In contrast, for $\tau = 2\tau_B$ the fidelity remains low. The degradation for large N values at large delay should be attributed to wavepacket dispersion due to anharmonicity. The simple solution is to apply the S pulse at $\tau = 0$ or τ_B . The choice $\tau = \tau_B$ is actually preferable since interference from the time-reversed (S,P) sequence at $\tau = 0$, as well as higher order processes (6-wave mixing etc.) not accounted for in our simulations, lead to smaller signal strength. Optimization of the *phases* of the S and P pulses (chirping) is another option that can be used for compensating for anharmonicity effects [18].

Discussion and Conclusions.— The CARS-QC proposal [4] is a promising new implementation of quantum logic, with potential near-term implications for quantum communication. Our main purpose in this work was to test the feasibility of this proposal by studying in detail the implementation of a benchmark quantum algorithm. We chose the Deutsch-Jozsa (DJ) problem for its conceptual and technical simplicity, and devised a modified algorithm that only requires quantum interference, not entanglement. This allowed us to directly test aspects related to the preparation of input vibrational superposition states and their dynamical evolution. To maintain fidelity, it is necessary to devise pulses that compensate for non-uniform Franck-Condon factors and counteract anharmonicity effects. These can be achieved through amplitude masking and frequency chirping, which can be optimally tailored for a given choice of delay between pulses. Here, we have indicated that intuitively obvious pulses already allow a clear demonstration of how quantum algorithms may be implemented in TFRCARS. The strategy in the laboratory demonstration of this, and similar algorithms involving rotation-vibration-electronic

qubits, will be to rely on genetic algorithms to design pulses optimized for particular tasks.

Acknowledgements.— DAL gratefully acknowledges support from NSERC. The QC effort at Irvine is supported through the US AFOSR, under grant F49620-01-1-0449.

TABLE I. Percentage Correlation/Distinguishability for DJ problem instances with different N and time delays τ . Last line (8t): “tailored” implementation.

-
- [1] D.G. Cory *et al.*, Fortschritte der Physik **48**, 875 (2000), and references therein.
 - [2] C. A. Sackett *et al.*, Nature **404**, 256 (2000), and references therein.
 - [3] A. Rauschenbeutel *et al.*, Phys. Rev. Lett. **83**, 5166 (1999), and references therein.
 - [4] R. Zadoyan, D. Kohen, D.A. Lidar, and V.A. Apkarian, Chem. Phys. **266**, 323 (2001).
 - [5] D. Deutsch and R. Jozsa, Proc. Roy. Soc. London Ser. A **439**, 553 (1992).
 - [6] I.L. Chuang *et al.*, Nature **393**, 143 (1998); J.A. Jones and M. Mosca, J. Chem. Phys. **109**, 1648 (1998); N. Linden *et al.*, Chem. Phys. Lett. **296**, 61 (1998); K. Dorai *et al.*, Phys. Rev. A **61**, 042306 (2000); R. Marx *et al.*, Phys. Rev. A **62**, 012310 (2000); D. Collins *et al.*, Phys. Rev. A **62**, 022304 (2000); J. Kim *et al.*, Phys. Rev. A **62**, 022312 (2000).
 - [7] S. Takeuchi, Phys. Rev. A **62**, 032301 (2000).
 - [8] J. Vala *et al.*, eprint quant-ph/0107058.
 - [9] S. Mukamel, *Principles of Nonlinear Optical Spectroscopy* (Oxford Univ. Press, Oxford, 1995).
 - [10] R. Zadoyan and V.A. Apkarian, Chem. Phys. Lett. **326**, 1 (2000), and references therein.
 - [11] D.P. DiVincenzo, Fortschritte der Physik **48**, 771 (2000).
 - [12] D. Deutsch *et al.*, Phys. Rev. Lett. **77**, 2818 (1996), erratum - *ibid.* **80**, 2022 (1998).
 - [13] S.A. Rice and M. Zhao, *Optical Control of Molecular Dynamics*, (John Wiley, NY, 2000).
 - [14] A.P. Peirce, M.A. Dahleh, and H. Rabitz, Phys. Rev. A **37**, 4950 (1988).
 - [15] R. Cleve *et al.*, Proc. Roy. Soc. London Ser. A **454**, 339 (1998).
 - [16] Our algorithm is similar to one described in D. Collins *et al.*, Phys. Rev. A **58**, R1633 (1998), except that it does not use a qubit tensor-product structure.
 - [17] D.T. Colbert and W.H. Miller, J. Chem. Phys. **96**, 1982 (1992).
 - [18] C.J. Bardeen *et al.*, J. Chem. Phys. **106**, 8486 (1997).

N	$\tau = 0$	$\tau = 1$	$\tau = 2$
4	99/86	99/90	99/85
6	95/79	95/78	91/69
8	84/60	84/62	73/41
8t	99/89	97/73	81/43

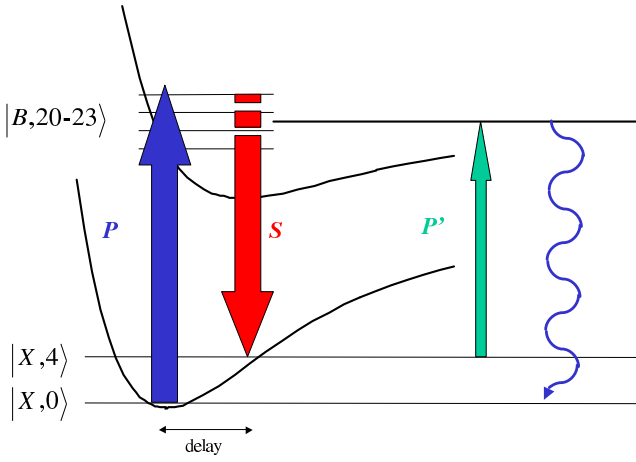


FIG. 1. X (ground) and B (excited) electronic potential energy surfaces of iodine, modelled as Morse potentials. Also shown: time-circuit diagram of pump (P), Stokes (S), and probe (P') pulses, and relevant vibrational states.

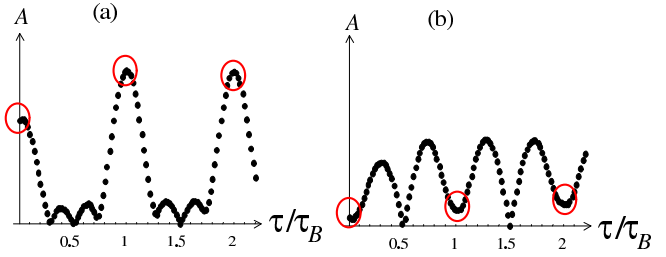


FIG. 3. Signal A as function of delay time τ for different masks. Time in units of (B) vibrational period. a) Constant function. b) Balanced function.

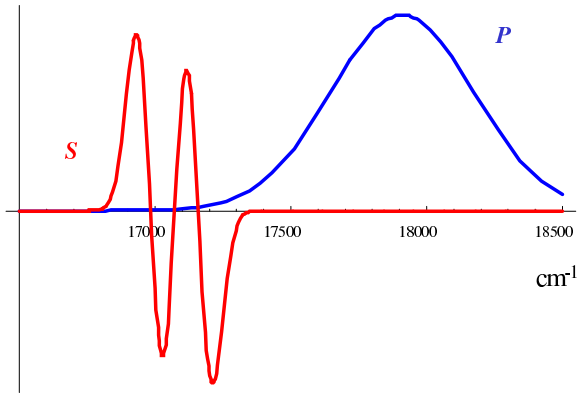


FIG. 2. Spectrum of P and S pulses. S pulse for (1,-1,1-1) mask is shown.

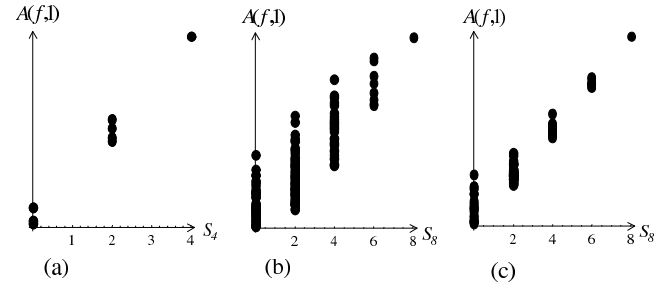


FIG. 4. Signal A as function of $S_N(f)$. a) $N = 4$, b) $N = 8$, c) "tailored" $N = 8$.